Int. J. Solids Structures Vol. 29, No. 10, pp. 1209–1219, 1992
Printed in Great Britain.

0020–7683/92 $5.00+.00

MODE JUMPING IN BIAXIALLY COMPRESSED PLATES

R. MAASKANT† and J. ROORDA
Department of Civil Engineering, University of Waterloo, Waterloo, Ontario, Canada N2L 3G1

(*Received* 17 *May* 1991; *in revised form* 5 *September* 1991)

Abstract—Interactive buckling in flat plates leads to the mode jumping phenomenon associated with secondary bifurcations in post-buckling. The behaviour of simply-supported plates under biaxial compression is investigated in detail and the nature of the interaction between buckling modes is described for a variety of loading conditions. The results provide the loading conditions under which qualitatively distinct post-buckling behaviour is observed. Stability boundaries are obtained for plates with initial imperfections.

1. INTRODUCTION

The buckling behaviour of plates has been studied extensively due to the important function which they serve as load-bearing components in a variety of thin-walled structures. The post-buckling behaviour of plates is stable and hence they remain structurally useful well beyond their critical buckling load. This contributes to their popularity and motivates detailed investigations of their post-buckling behaviour.

Experiments on plates have revealed that changes in the buckled form occur as loading progresses. Supple and Chilver (1967) identify these as minor and major modifications of the buckled form, the latter of which is the subject of the current investigation. Major modifications of form often occur suddenly in experiments and may consist of a dynamic snap from one buckled form to another involving a different number of longitudinal and transverse half-waves [see for example Ojalvo and Hull (1958), Sharman and Humpherson (1968) and Stein (1959)]. Analysis of the plate post-buckling behaviour [e.g. Dombourian *et al.* (1976), Nakamura and Uetani (1979), Supple (1970), Uemura and Byon (1977)] has revealed that secondary bifurcations associated with the mode jumping phenomenon exist on the post-buckling equilibrium path of plates.

The present study seeks to shed light on the mode jumping phenomenon by considering the two mode interaction of simply-supported plates under biaxial loading. For arbitrary (piecewise linear) loading paths it is shown how qualitatively distinct post-buckling behaviour may arise. Two particular loading situations are considered, first, applied edge displacements, and second, uniaxial loading with in-plane elastic restraints on the unloaded edges. These include as special cases the examples studied by Supple (1970) in which the unloaded edges of a uniaxially loaded plate are alternatively free and fixed with respect to transverse in-plane displacement. The analysis illustrates the influence of the loading conditions on the mode jumping phenomenon.

2. POST-BUCKLING ANALYSIS

Consider a rectangular plate of thickness t and in-plane dimensions $l \times b$ in the direction of the x and y axis, respectively (the origin of which is at the centre of the plate). The plate material is isotropic with Young's modulus E and Poisson's ratio ν. For the purposes of the present study it is sufficient to consider the interaction between a pair of buckling modes of the form:

†Presently, Research Associate, Institute for Aerospace Studies, University of Toronto, 4925 Dufferin St., Downsview, Ontario, Canada M3H 5T6.

$$w(x, y) = t \cos \frac{\pi y}{b}\left(u_m \sin \frac{m\pi x}{l} + u_n \cos \frac{n\pi x}{l}\right) \tag{1}$$

$$w_0(x, y) = t \cos \frac{\pi y}{b}\left(a_m \sin \frac{m\pi x}{l} + a_n \cos \frac{n\pi x}{l}\right), \tag{2}$$

where w and w_0 are the total and initial out-of-plane displacements of the plate, both of which are measured from the mid-plane of the flat configuration. This displacement pattern is deemed to be appropriate for the present case of biaxial loading when $l > b$ and for some minimal restrictions on the load path. To satisfy the simply-supported boundary conditions m must be even and n must be odd but this is not particularly restrictive since the interaction of successive buckling modes is of interest here. The assumed in-plane boundary conditions correspond to straight, parallel but otherwise unrestrained edges.

The potential function for the plate can be derived using the above assumed displacements in conjunction with the solution of the well known von Kármán large deflection compatibility equation as provided by Supple (1970). The resulting (non-dimensionalized) potential function is

$$P = \tfrac{1}{4}(A_m u_m^4 + 2A_{mn} u_m^2 u_n^2 + A_n u_n^4) + \tfrac{1}{2}(\Lambda_m^0 - m^2\Lambda^1 - \Lambda^2)u_m^2 + \tfrac{1}{2}(\Lambda_n^0 - n^2\Lambda^1 - \Lambda^2)u_m^2 - \Lambda_m^0 a_m u_m - \Lambda_n^0 a_n u_n, \tag{3}$$

in which

$$A_k = \frac{3(1-\nu^2)}{16\gamma^2}(k^4+\gamma^4), \quad k = m, n$$

$$A_{mn} = \frac{3(1-\nu^2)}{16\gamma^2}[4\gamma^4 + m^2n^2 + \gamma^4(m-n)^2\alpha_{mn} + \gamma^4(m+n)^2\beta_{mn}]$$

$$\alpha_{mn} = \frac{(m-n)^2}{[(m+n)^2+4\gamma^2]^2}$$

$$\beta_{mn} = \frac{(m+n)^2}{[(m-n)^2+4\gamma^2]^2}$$

$$\Lambda_k^0 = \frac{(k^2+\gamma^2)^2}{4\gamma^2}, \quad k = m, n$$

$$\Lambda^1 = \frac{\sigma_1 b^2 t}{4\pi^2 D}, \quad \Lambda^2 = \frac{\sigma_2 l^2 t}{4\pi^2 D},$$

and $\gamma = l/b$ is the aspect ratio of the plate. The non-dimensional loading parameters Λ^1, Λ^2 correspond to the compressive in-plane edge stresses σ_1, σ_2 in the x and y directions respectively. It can be observed that the above potential energy expression, in the absence of initial imperfections (i.e. $a_m = a_n = 0$), is an even function of the non-dimensional displacement coordinates u_1, u_2. In the general theory of elastic stability as described by Thompson and Hunt (1984) such systems are termed doubly symmetric. The buckling behaviour, available from previous studies [e.g. Supple (1967, 1968), Wicks (1988)], is now described in the context of biaxial loading.

The principle of stationary potential energy leads to the equilibrium equations:

$$u_m[A_m u_m^2 + A_{mn} u_n^2 + \Lambda_m^0 - m^2\Lambda^1 - \Lambda^2] - \Lambda_m^0 a_m = 0, \tag{4}$$

$$u_n[A_n u_n^2 + A_{mn} u_m^2 + \Lambda_n^0 - n^2\Lambda^1 - \Lambda^2] - \Lambda_n^0 a_n = 0, \tag{5}$$

and, for the perfect plate ($a_m = a_n = 0$), the vanishing of the second variation of the potential energy yields the critical loads:

$$m^2\Lambda^1 + \Lambda^2 = \Lambda_m^0 \tag{6}$$

$$n^2\Lambda^1 + \Lambda^2 = \Lambda_n^0, \tag{7}$$

for buckling into the uncoupled u_m and u_n modes respectively. These are termed *characteristic lines*, parts of which form the stability boundary in the two-dimensional load space (Λ^1, Λ^2). These can be written in terms of a single loading parameter along a particular loading path of interest. Consider a path in the two-dimensional load space which emanates from a fundamental equilibrium state F. The subsequent loading is assumed to occur along a load ray at an angle ϕ counterclockwise from the Λ^1 axis and progress from the point F is measured by the parameter λ. It is assumed that F is within or on the stability boundary defined by eqns (6) and (7) such that by the uniqueness of the prebuckling states, the loading path leading to F may be arbitrarily specified. The subsequent loading ray is here confined to directions toward the region of instability with respect to the participating modes u_m and u_n. The loading terms in the above may then be written:

$$\Lambda_k^0 - k^2\Lambda^1 - \Lambda^2 = B_k(\lambda_k^F - \lambda), \tag{8}$$

where

$$B_k = k^2\cos\phi + \sin\phi$$

$$\lambda_k^F = (\Lambda_k^0 - k^2\Lambda^{1^F} - \Lambda^{2^F})/B_k,$$

for $k = m, n$. The superscript F denotes evaluation at the fundamental equilibrium state F.

A classification of the post-buckling behaviour is now given for the perfect plate. Setting the initial imperfections a_m, a_n to zero, there exist two uncoupled equilibrium solutions:

$$u_n = 0, \quad A_m u_m^2 + B_m(\lambda_m^F - \lambda) = 0 \tag{9}$$

$$u_m = 0, \quad A_n u_n^2 + B_n(\lambda_n^F - \lambda) = 0, \tag{10}$$

which are termed *primary* buckling paths since they bifurcate from the fundamental equilibrium path $u_m = u_n = 0$. These are stable symmetric equilibrium paths, familiar in plate post-buckling. Added to these is a *secondary* solution which bifurcates from the primary mode(s). It involves both displacement coordinates and is given by

$$Fu_m^2 + Gu_n^2 = H, \tag{11}$$

where

$$F = A_m B_n - A_{mn} B_m$$

$$G = A_{mn} B_n - A_n B_m$$

$$H = B_m B_n(\lambda_n^F - \lambda_m^F).$$

This coupled solution takes the form of a hyperbola or an ellipse centred at the origin in u_m–u_n space. In the λ–u_m and λ–u_n planes the coupled solutions are parabolic, given by

$$(A_m A_n - (A_{mn})^2)u_m^2 + G\lambda + A_n B_m \lambda_m^F - A_{mn} B_n \lambda_n^F = 0 \tag{12}$$

$$(A_m A_n - (A_{mn})^2)u_n^2 - F\lambda + A_m B_n \lambda_n^F - A_{mn} B_m \lambda_m^F = 0. \tag{13}$$

The coupled solution therefore bifurcates symmetrically from one of the uncoupled solutions in the case of the hyperbolic form and from both uncoupled solutions when (11) is elliptic. Of particular interest is the secondary bifurcation from the lower uncoupled path since that path is stable initially. The uncoupled mode then loses its stability and the subsequent secondary branching is stable or unstable according to the sign of the curvature in (12) or (13).

The form of secondary branching depends on the signs of F and G for which there are four possibilities:

$$\left.\begin{array}{lll} \text{(i)} & F>0, & G<0 \\ \text{(ii)} & F<0, & G>0 \\ \text{(iii)} & F>0, & G>0 \\ \text{(iv)} & F<0, & G<0 \end{array}\right\}. \tag{14}$$

The first two give the hyperbolic form while the latter two correspond to the elliptic form; these are illustrated in Fig. 1. The signs of F and G depend solely on the loading angle ϕ while the sign of H in eqn (11) is dependent on the order of occurrence of the u_m and u_n primary bifurcations along the loading path. When $H>0$ the u_m mode will be the initial (or lower) buckling mode, and when $H<0$ the u_n mode is the initial buckling mode. The hyperbola of (14i) branches from the lower uncoupled path and that of (14ii) branches from the upper uncoupled path. The ellipses of (14iii) and (14iv) exist only for $H>0$ and $H<0$ respectively. When $H=0$, eqn (11) gives the degenerate form of the hyperbola consisting of the pair of asymptotes, and the elliptic form collapses to the origin.

The dependence of the forms of buckling of (14) on the direction of loading is easily determined. Because of the restriction that the loading is to be directed toward the region of instability, the coefficients B_m, B_n are always positive. In the present plate buckling problem, the coefficients A_m, A_n, A_{mn} are also positive so that the classification given by the inequalities (14) can be determined in terms of the loading direction according to

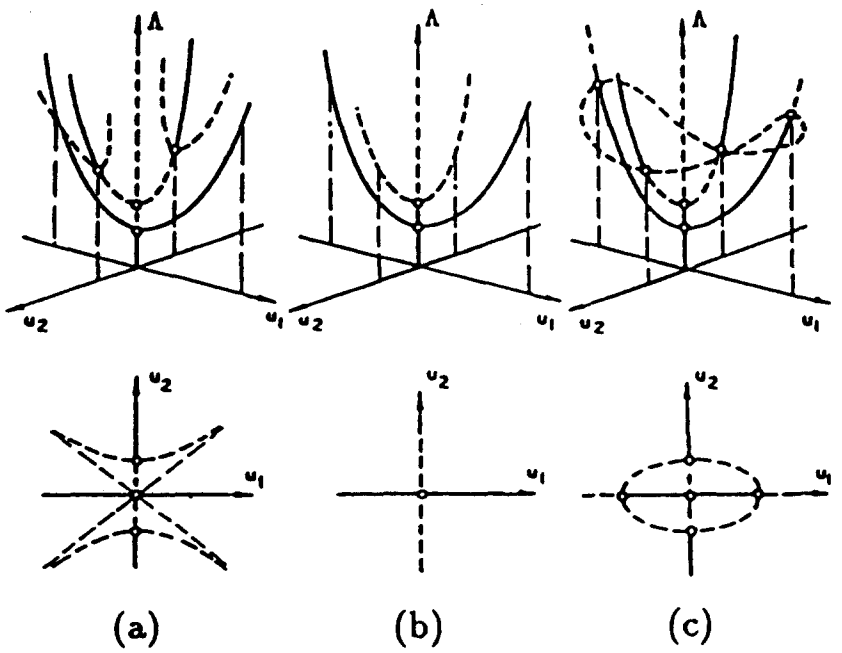

Fig. 1. Forms of doubly symmetric buckling [reproduced from Supple (1968)]. (a) Hyperbola branching from upper uncoupled mode. (b) No coupled solution. (c) Ellipse.

$$\left.\begin{array}{ll} \text{(i)} & A_{mn}/A_n < B_m/B_n < A_m/A_{mn} \\ \text{(ii)} & A_m/A_{mn} < B_m/B_n < A_{mn}/A_n \\ \text{(iii)} & B_m/B_n < \min\,(A_m/A_{mn},\ A_{mn}/A_n) \\ \text{(iv)} & B_m/B_n > \max\,(A_m/A_{mn},\ A_{mn}/A_n) \end{array}\right\}. \tag{15}$$

in which the ratio B_m/B_n is a function of ϕ. It is evident that three regions of loading will be identified consisting of a region of hyperbolic secondary branching bounded by two regions of elliptic secondary branching. This will be illustrated in the example in the following section.

The curvatures of the coupled paths in the λ–u_m and λ–u_n planes, important for stability considerations, can be established on the basis of the coupled form once the sign of bracketed terms in eqns (12) and (13) are known. The intuitive result that the signs of the curvatures are the same in the hyperbolic case and opposite for the elliptic form can thereby be verified.

It is of interest to obtain the loci in load space which correspond to critical buckling configurations for the imperfect plate. For this purpose the vanishing of the stability determinant

$$\left|\frac{\partial^2 P}{\partial u_i\,\partial u_j}\right| = 0, \tag{16}$$

leads to

$$[3A_m u_m^2 + A_{mn}u_n^2 + B_m(\lambda_m^F - \lambda)][3A_n u_n^2 + A_{mn}u_m^2 + B_n(\lambda_n^F - \lambda)] - 2A_{mn}u_m u_n = 0. \tag{17}$$

The solution of this equation in conjunction with the equilibrium eqns (4) and (5) will yield the critical equilibrium states. This has been worked out elsewhere for systems of a similar form [e.g. Roorda and Reis (1977), Supple (1968), Wicks (1988)] and yields imperfection sensitivity surfaces in the space of (λ, a_m, a_n). The points on these surfaces represent limit points and bifurcations on the equilibrium paths of the imperfect structure. In the present context, these imperfection sensitivity surfaces correspond to the particular load path associated with λ.

Attention is restricted to nonzero imperfections in each of the modes, separately and in turn. It is evident from the equilibrium equations that the equilibrium path in these cases will be initially uncoupled, that is, it will only involve displacements in the form of the initial imperfection. Thus, the last term in the criticality condition (17) is zero. It can be shown that the first of the remaining terms is associated with a symmetric bifurcation with respect to the u_m displacement coordinate for the initial imperfections $a_m = 0$, $a_n \neq 0$ and the second represents a symmetric bifurcation with respect to u_n for $a_m \neq 0$, $a_n = 0$.

3. EXAMPLES

Some numerical results are now presented for a plate with aspect ratio $\gamma = 2$. Consideration of a more general form of buckling than that of eqn (1) indicates that modes with more than a single transverse half-wave occur at much higher compressive load levels [see Timoshenko and Gere (1961)]. Therefore the assumed buckling mode is deemed to be sufficient.

The stability boundary for the perfect plate is shown in Fig. 2 by the solid lines and the extensions of these characteristic lines into the post-buckling region is shown by dashed lines. Proceeding clockwise from the Λ^2 axis, the lines comprising the stability boundary correspond to buckling into a single transverse half wave and 1, 2 and 3 longitudinal half-waves, respectively. For the two mode interaction considered here, the participating modes are the critical mode and the next primary mode encountered along the particular loading path of interest.

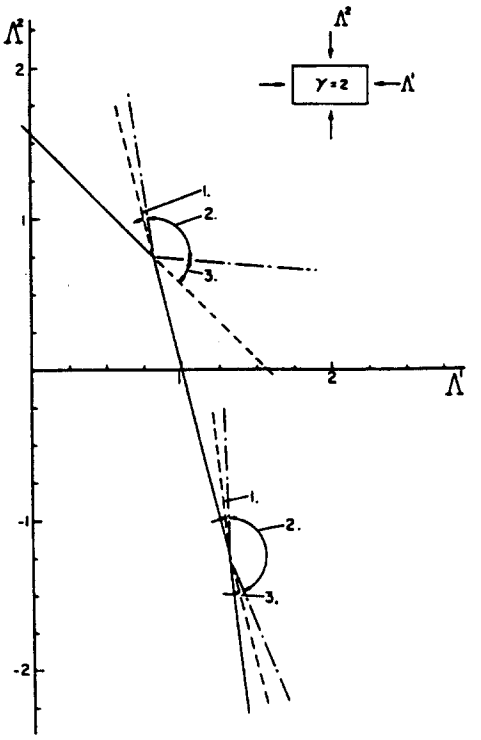

Fig. 2. Loading directions for: 1. no (elliptic) coupled solution, 2. hyperbolic coupled solution, 3. elliptic (no) coupled solution.

Loading rays defining the transition between different forms of coupled buckling solutions are calculated from the inequalities of (15) and are illustrated in Fig. 2. The limiting angles so calculated are dependent on the contributing mode numbers m and n but not on the order in which they occur along the load path. The corresponding limiting load rays are therefore shown at the coincident buckling point, although, with some further interpretation, they are seen to be valid at any point on the adjoining primary characteristic lines. For both the u_1–u_2 and the u_2–u_3 interaction, the region of permissible loading directions is divided into three regions. In both cases the central loading region corresponds to hyperbolic secondary branching and the outer regions correspond to an elliptic secondary equilibrium path. The hyperbolic branching occurs in every case from the upper primary equilibrium path. The interpretation of the elliptic buckling regions is dependent on the order of occurrence of the primary modes as was noted in the previous section. For u_1–u_2 interaction and a loading path which first intersects the u_1 stability boundary, region 1 of Fig. 2 corresponds to the imaginary form of the ellipse such that no secondary branching occurs while loading rays in the direction of region 3 load to an elliptic secondary equilibrium path. When the u_2 stability boundary is intersected first, the interpretation is interchanged such that for region 1 the elliptic secondary equilibrium path exists and for region 3 there is no secondary branching.

The initial curvature of the secondary equilibrium paths is of interest in relation to stability considerations. This is easily calculated from eqns (12) and (13) from which it is found that the sign of the curvature of the projection onto the λ–u_m and λ–u_n planes is the same as that of G and $-F$, respectively. In all cases the hyperbolic form has positive curvature in both projections but these curvatures are of opposite sign for the elliptic form. In the latter case, the curvature of the coupled solution branching from the lower primary mode is always negative. The implication of this is that the post-buckling equilibrium path of the plate becomes unstable at a secondary bifurcation point such that a change in the buckled form of the plate occurs. This is often termed mode jumping since for dead loading the instability of the secondary path leads to snap-through buckling from the primary post-buckling path.

In order to realize changes in the form of the coupled buckling solution as described above, different loading scenarios are now considered. A plate element may be loaded, either experimentally or in the context of some structural system, by controlling the magnitude of the loads directly, or indirectly via a rigid or semi-rigid loading device whereby displacements are prescribed.

It is evident from Fig. 2 that for a continuous straight load ray from the origin (i.e. proportional loading) the coupled solution will always be of the hyperbolic form and secondary branching (for the perfect system at least) is innocuous. In a rigid loading situation in which proportional in-plane displacments of the plate edges are imposed, the sudden change from the pre-buckling to the post-buckling in-plane stiffness can be expected to bring about a change in direction of the loading ray at the critical point. Such a loading ray may be deflected to such an extent that it enters the regime of elliptic buckling. This type of loading is now considered where

$$\frac{\Delta v}{\Delta u} = \eta \text{ (constant)}, \tag{18}$$

and

$$\Delta u = \int_{-l/2}^{l/2} u_{,x}\, \mathrm{d}x, \quad \Delta v = \int_{-b/2}^{b/2} v_{,y}\, \mathrm{d}y.$$

Substituting the required displacement gradients, available from the non-linear strain–displacement relations, eqn (18) yields a linear relationship between the loads, which for the pre-buckling states is

$$\frac{\Lambda^2}{\Lambda^1} = \frac{\gamma^2(\eta\gamma + \nu)}{1 + \nu\eta\gamma}, \tag{19}$$

and for post-buckling is

$$\gamma^2(\eta\gamma + \nu)\Lambda^1 - (1 + \nu\eta\gamma)\Lambda^2 + \tfrac{1}{8}\gamma(1 - \nu^2) \times [(\eta m^2 - \gamma)u_m^2 + (\eta n^2 - \gamma)u_n^2] = 0. \tag{20}$$

When uncoupled buckling occurs with respect to the coordinate u_k, the above yields the load ray:

$$\frac{\mathrm{d}\Lambda^2}{\mathrm{d}\Lambda^1} = \frac{8A_k\gamma^2(\eta\gamma + \nu) - 3\gamma k^2(1 - \nu^2)(\gamma - \eta k^2)}{8A_k(1 + \nu\eta\gamma) + 3\gamma(1 - \nu^2)(\gamma - \eta k^2)}. \tag{21}$$

Along the coupled equilibrium path the projection onto the load plane can also be calculated using eqn (20). Thus, each mode of buckling has a different associated in-plane stiffness which causes the path followed in load space to change in direction at its associated point of bifurcation. For example, consider a loading which results in the elliptic form of coupled buckling. Loading initially progresses along the load ray given by eqn (19), illustrated in Fig. 3. A bifurcation occurs at C and subsequent loading is along the *deflected ray* of eqn

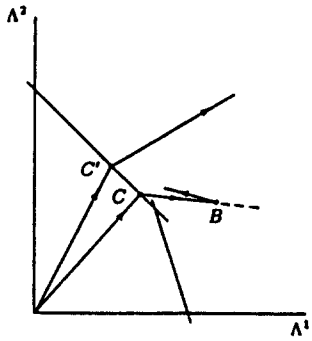

Fig. 3. Example loading paths for displacement controlled loading.

(21). The secondary bifurcation at B causes another shift of the load ray which can be calculated from eqn (20). Since the load decreases along this bifurcated path, the loading reverses direction. If the coupled buckling form is hyperbolic, the bifurcation B does not occur during natural loading since the secondary branching is from the higher uncoupled mode. The *post-buckling load ray* is then given by eqn (21) alone as illustrated by the loading through C' in Fig. 3.

Illustrated in Fig. 4 are the loading rays for some cases of proportional applied edge displacements. The loading paths defining the transition from the hyperbolic to the elliptic form have also been identified. The load ray $\eta = 0$, corresponding to longitudinal edges held rigidly apart, exhibits the elliptic form of coupled buckling with $n = 1$, $m = 2$ as was reported by Supple (1970). It can be observed that the u_1, u_2 coupling does not occur when the initial bifurcation point C is on $u_2 = 2$ stability boundary. Upon buckling into the u_2 mode, the load ray deflects quite severely with the result that during subsequent loading it is directed within the region of stability with respect to u_1. It can be shown that the u_2 uncoupled equilibrium path remains stable with respect to u_1 so that secondary buckling involving u_1 is precluded. Interaction therefore occurs with the u_3 uncoupled mode. The load ray for which coincident u_1 and u_2 buckling occurs ($\eta = \eta_2$ in Fig. 4) is shown with two post-buckling load rays. One of these corresponds to the u_1 mode and the more severely deflected one corresponds to the u_2 mode. A further possibility must be investigated corresponding to the degenerate hyperbolic form of coupled buckling which occurs for coincident buckling. It is intuitively evident [and can be verified using eqn (20)] that the load ray corresponding to such a coupled solution must lie in the region between the u_1 and u_2 load rays since it will have stiffness characteristics intermediate to the two contributing modes. Thus it lies in the elliptic region for which no such solution exists and the possibility of a coupled path emanating from the coincident point is eliminated. The equilibrium path actually followed by the structure when $\eta = \eta_2$ is the stable u_2 path.

Another type of loading which may be encountered is uniaxial load application with the plate restrained elastically in the transverse direction along its longitudinal edges such that

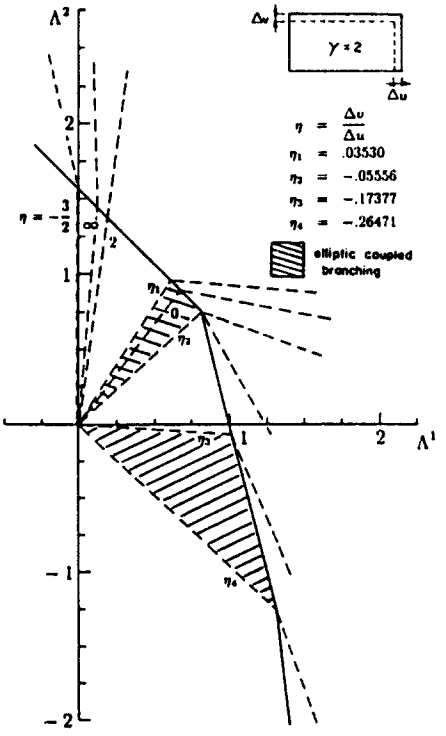

Fig. 4. Loading paths for applied displacement ratio η.

$$\sigma_2 = \mu E \Delta v / b, \tag{22}$$

the constant μ defining the relative stiffness of the edge restraint. The projection of the equilibrium path onto load space will follow the relation:

$$\nu\Lambda^1 - \Lambda^2 \frac{1+\mu}{\gamma^2 \mu} - \tfrac{1}{8}(1-\nu^2)(u_m^2 + u_n^2) = 0, \tag{23}$$

for which the pre-buckling load ray is

$$\frac{\Lambda^2}{\Lambda^1} = \frac{\mu \nu \gamma^2}{1+\mu}. \tag{24}$$

The post-buckling ray for the uncoupled u_k mode is

$$\frac{d\Lambda^2}{d\Lambda^1} = \frac{\mu\gamma^2[8A_k\nu - 3(1-\nu^2)k^2]}{8A_k(1+\mu) + 3\mu\gamma^2(1-\nu^2)}. \tag{25}$$

This case is illustrated in Fig. 5 where the boundaries of the different coupling behaviours are illustrated. For $\mu \in [0, \mu_2]$, μ_2–μ_3 interaction occurs and for $\mu \in (\mu_1, \infty)$ interaction occurs between the u_1 and u_2 modes. The branching behaviour is of the hyperbolic type from the upper primary uncoupled path except for very stiff transverse restraint.

Numerical results for the loci of critical loads of imperfect plates are shown in Fig. 6. The solid lines represent the symmetric bifurcations (s.b.) indicated when the associated initial imperfection is nonzero. The dash-dot lines represent the secondary bifurcations involving these modes for the perfect plate. For load rays corresponding to the hyperbolic form of secondary branching (for the perfect plate) buckling occurs only when the plate imperfection is in the form of the second primary mode. For load rays associated with the nondegenerate elliptic form (for the perfect plate) buckling occurs for plate imperfections in the form of the first primary mode. Note that the first and second primary mode refer to the modes encountered along the load path of interest. The nature of the buckling behaviour for any one of the imperfections indicated can be most easily established with reference to the behaviour of the perfect system. Having determined this behaviour for the loading path of interest, previous studies [e.g. Supple (1970), Wicks (1988)] can be consulted for the relation between the behaviour of the perfect and the imperfect system.

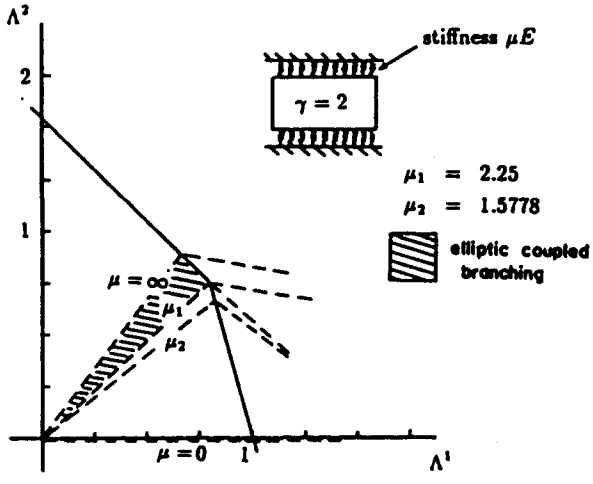

Fig. 5. Loading paths for elastically restrained longitudinal edges.

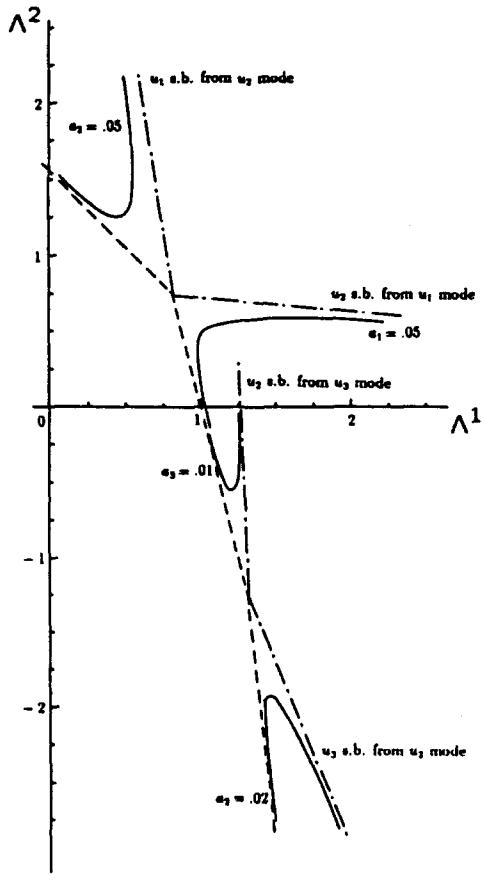

Fig. 6. Stability boundaries for imperfect plate.

4. DISCUSSION

Simply-supported rectangular plates under the action of biaxial in-plane loads have been considered. The qualitative behaviour of the ideal plate has been found to be particularly sensitive to the manner in which the loads are applied. Different loading scenarios for which there is a degree of in-plane displacement control illustrate the manner in which such qualitative changes in behaviour may occur. Although such idealized plates do not exist, their behaviour forms a basis from which the behaviour of more realistic imperfect plates is more clearly understood. In this regard the present results should be considered in the light of previous studies where this relationship is described [e.g. Supple (1970, 1968), Thompson and Hunt (1984), Wicks (1988)].

It is evident from the literature cited earlier that higher modes and possibly combinations of these modes must be considered to obtain a more complete picture of the mode jumping phenomenon. This would appear to be more important for loading rays (or plate aspect ratios) for which a number of primary critical points approach each other. Such considerations are also necessary in the case of no coupled branching from the lower primary equilibrium path identified by the present analysis. There is evidence of secondary branching in these cases when interaction with other buckling modes is considered. These occur at relatively high loads and appear to be related to coupling with higher modes as well as to the minor changes which occur in the primary mode in advanced post-buckling.

REFERENCES

Dombourian, E. M., Smith, C. V. and Carlson, R. L. (1976). A perturbation solution to a plate post-buckling problem. *Int. J. Non-Linear Mech.* **11**, 49–58.

Nakamura, T. and Uetani, K. (1979). The secondary buckling and post-secondary buckling behaviours of rectangular plates. *Int. J. Mech. Sci.* **21**, 265–286.

Ojalvo, M. and Hull, F. H. (1958). Effective width of thin rectangular plates. *ASCE, J. Engng Mech. Div.* **84**, p. 1718.

Roorda, J. and Reis, A. J. (1977). Non-linear interactive buckling: sensitivity and optimality. *J. Struct. Mech.* **5**, 207–232.

Sharman, P. W. and Humpherson, J. G. (1968). An experimental and theoretical investigation of simply supported thin plates subjected to lateral loads and uniaxial compression. *Aeronaut. J. Roy. Aeronaut. Soc.* **72**, 431–436.

Stein, M. (1959). Loads and deformations of buckled rectangular plates. NASA Technical Report, R-40.

Supple, W. J. (1967). Coupled branching configurations in the elastic buckling of symmetric structural systems. *Int. J. Mech. Sci.* **9**, 97–112.

Supple, W. J. (1968). On the change in buckle pattern in elastic structures. *Int. J. Mech. Sci.* **10**, 737–745.

Supple, W. J. (1970). Changes of waveform of plates in the post-buckling range. *Int. J. Solids Structures* **6**, 1243–1258.

Supple, W. J. and Chilver, A. H. (1967). Elastic post-buckling of compressed rectangular plates. In *Thin-walled Structures* (Edited by A. H. Chilver), pp. 136–152. Chatto and Windus, London.

Thompson, J. M. T. and Hunt, G. W. (1984). *Elastic instability Phenomenon*. Wiley, New York.

Timoshenko, S. and Gere, J. M. (1961). *Theory of Elastic Stability*. McGraw-Hill, New York.

Uemura, M. and Byon, O. (1977). Secondary buckling of a flat plate under uniaxial compression Part 1: Theoretical analysis of simply supported flat plate. *Int. J. Non-Lin. Mech.* **12**, 355–370.

Wicks, P. J. (1988). A classification of behaviour in doubly-symmetric compound branching. *Int. J. Non-Lin. Mech.* **30**, 821–833.